HHS Public Access

Author manuscript

Neuron. Author manuscript; available in PMC 2017 May 04.

Published in final edited form as:

Neuron. 2016 May 4; 90(3): 635–648. doi:10.1016/j.neuron.2016.03.031.

The basal forebrain and motor cortex provide convergent yet distinct movement-related inputs to the auditory cortex

Anders Nelson[1] and **Richard Mooney**[1,*]

[1]Department of Neurobiology, Duke University Medical Center, Durham, NC, 27710, USA

Summary

Cholinergic inputs to the auditory cortex from the basal forebrain (BF) are important to auditory processing and plasticity, but little is known about the organization of these synapses onto different auditory cortical neuron types, how they influence auditory responsiveness, and their activity patterns during various behaviors. Using intersectional tracing, optogenetic circuit mapping, and in vivo calcium imaging, we found that cholinergic axons arising from the caudal BF target major excitatory and inhibitory auditory cortical cell types, rapidly modulate auditory cortical tuning, and display fast movement-related activity. Furthermore, the BF and the motor cortex – another source of movement-related activity – provide convergent input onto some of the same auditory cortical neurons. Cholinergic and motor cortical afferents to the auditory cortex display distinct activity patterns and presynaptic partners, indicating that the auditory cortex integrates bottom-up cholinergic signals related to ongoing movements and arousal with top-down information concerning impending movements and motor planning.

Introduction

Sensory processing involves the integration of sensory inputs with a variety of other signals that convey information about internal state, including attention, arousal, and motor planning. The auditory cortex (ACtx) is a major site of such integration, receiving ascending auditory inputs and also a wide range of cortical and subcortical inputs that are implicated in movement- and state-dependent auditory processing, attention, and learning (Budinger et al., 2008; Eliades and Wang, 2003; Froemke et al., 2007; Kilgard and Merzenich, 1998; Letzkus et al., 2011; Polley et al., 2006). For example, auditory cortical responses are suppressed during a wide range of movements, and a component of this modulation is driven by neurons in the secondary motor cortex that extend axon collaterals to ACtx ($M2_{ACtx}$ neurons), where they make fast excitatory synapses on inhibitory interneurons and pyramidal cells (Nelson et al., 2013; Schneider et al., 2014). ACtx also receives neuromodulatory inputs, including cholinergic inputs arising from the basal forebrain (BF). BF signaling has been implicated in

* Correspondence: mooney@neuro.duke.edu.

Author Contributions

A.N and R.M. designed experiments. A.N. performed and analyzed all experiments. A.N. and R.M. wrote the paper.

mediating more rapid effects on auditory cortical activity (Johnston et al., 1981; McKenna et al., 1989), including those associated with attention and arousal (Everitt and Robbins, 1997; Hangya et al., 2015; Metherate et al., 1992; Sarter et al., 2005), as well as slower effects, such as the long term facilitation of auditory responses (Bakin and Weinberger, 1996; Froemke et al., 2007; Kilgard and Merzenich, 1998). Intriguingly, cholinergic inputs in other sensory systems can convey movement-related information (Eggermann et al., 2014; Fu et al., 2014; Lee et al., 2014; Pinto et al., 2013), which may enable them to rapidly modulate sensory processing in a state- or task-dependent manner. In ACtx, the capacity of cholinergic inputs to convey movement-related signals that converge closely in space and time with those arising from the motor cortex could also underlie the more gradual modification of response properties that can accompany the learning of new sensorimotor associations.

Despite the important role that cholinergic inputs to ACtx play in auditory processing and plasticity, the organization of cholinergic synapses on different auditory cortical neuron types remains poorly understood (Munoz and Rudy, 2014). Furthermore, how cholinergic terminals modulate auditory cortical responses and the types of signals they convey during active behaviors remains largely unexplored. Finally, the extent to which cholinergic and motor cortical terminals converge in ACtx remains unclear. Resolving these issues is critical for understanding how ACtx integrates different internal signals to facilitate auditory processing and guide auditory learning.

One challenge to addressing these issues is that cholinergic and non-cholinergic projection neurons are interspersed in the BF, making the selective manipulation and monitoring of cholinergic projections to ACtx difficult to achieve (Kalmbach et al., 2012; Zaborszky and Duque, 2000; Zaborszky et al., 1999). And although studies that combine electrophysiological recordings from identified auditory cortical cell types with pharmacological manipulations have provided useful insights, including the effects of activating different types of cholinergic receptors on auditory cortical excitability (Kawaguchi, 1997; Munoz and Rudy, 2014; Nunez et al., 2012; Poorthuis et al., 2013), they cannot address how endogenous release of transmitter from BF terminals modulates auditory cortical activity. Finally, the high-resolution imaging methods necessary to measure cholinergic terminal activity have yet to be applied in ACtx. Here we overcame these challenges by using intersectional rabies tracing methods, in vitro and in vivo optogenetic manipulation of cholinergic BF terminals in ACtx, and in vivo imaging of BF terminals in ACtx of active, head-fixed mice.

Results

SIn_{ACh} neurons innervate four major auditory cortical neuron types

To determine which auditory cortical cell types receive direct input from the BF, we conducted a series of deficient rabies-based trans-synaptic tracing experiments targeted to auditory cortical inhibitory neurons expressing PV, SST, or VIP, or to auditory cortical excitatory neurons expressing CaMKII (Wickersham et al., 2007a; Wickersham et al., 2007b). We injected two Cre recombinase-dependent adeno-associated viruses (AAVs) -- one expressing the avian receptor for the EnVA glycoprotein (TVA) fused to mCherry (AAV-FLEX-TVA-mCherry) and the other expressing the rabies glycoprotein (AAV-FLEX-RG) --

into the primary auditory cortex (ACtx) of PV-Cre, SST-Cre, VIP-Cre, or CaMKII-Cre mice (Figure 1A). After waiting two weeks for TVA-mCherry and RG to be expressed in the target cell type, we then injected EnVA-pseudotyped RG-deficient rabies virus expressing GFP (EnVA-RΔG-GFP) into ACtx (Figure 1B). This virus selectively infects neurons expressing TVA (starter cells), and the virus's RG deficiency is complemented in the subset of starter cells that also express RG. Consequently, rabies virus-GFP is manufactured and shed by this subset of starter neurons, resulting in the subsequent expression of GFP in their presynaptic partners (Figure 1C). We confirmed our injections were correctly targeted by the expression of TVA-mCherry in ACtx, and by GFP expression in the ipsilateral auditory thalamus (MGB) and contralateral ACtx, and other brain regions that are known from prior studies to supply afferents to ACtx (Figure 1D-G; Supplemental Figure 1A-F; Supplemental Table 1) (Budinger et al., 2008; Nelson et al., 2013).

These rabies-based trans-synaptic tracing experiments revealed that all four major auditory cortical neuron types receive input from a dispersed population of magnocellular neurons in the substantia innominata complex (SIn) of the caudal BF (Figure 1H-K). Reconstructing and superimposing the locations of GFP-expressing SIn neurons in different PV-Cre, SST-Cre, VIP-Cre, or CaMKII-Cre mice revealed extensive overlap in their spatial distributions (Figure 1L, M; n = 2 mice per group). Furthermore, similarly large proportions of SIn neurons that innervated the different auditory cortical neuron types were immunopositive for choline acetyltransferase (ChAT) (Figure 1N, O; CaMKII: 82.2 ± 7.3%, n = 3 mice; PV: 87.9 ± 5.6%, n = 2 mice; VIP: 68.6 ± 8.1%, n = 3 mice, SST: 87.0 ± 9.2%, n = 3 mice; p = 0.598). Intracellular staining and whole-cell current clamp recordings from identified auditory cortical-projecting SIn neurons confirmed that these neurons were $ChAT^+$ and displayed intrinsic properties previously described for two physiologically distinct classes of cholinergic SIn neurons (Supplemental Figure 1G-L; n = 7 neurons from 3 mice)(Hedrick and Waters, 2010; Unal et al., 2012). We also found close appositions between cholinergic SIn axons (labeled by injecting AAV-FLEX-GFP into SIn of ChAT-Cre mice) and the somata and dendrites of multiple ACtx cell types (Supplemental Figure 2A-D; n = 2 mice). Therefore, cholinergic neurons in SIn innervate four major auditory cortical neuron types.

SIn axons evoke excitatory and inhibitory currents in ACtx neurons

We combined an intersectional optogenetic strategy and whole-cell voltage clamp recordings in brain slices to characterize the physiological properties of the synapses that cholinergic SIn axons make with auditory cortical neurons (Figure 2A). We injected AAV-FLEX-ChR2 in SIn of ChAT-Cre mice, which resulted several weeks later in the widespread expression of ChR2 in SIn_{ACh} axon terminals in ACtx (Figure 2B-D). We then made whole-cell voltage clamp recordings from neurons across different layers of ACtx in acute coronal brain slices; neurons were classified as pyramidal neurons or interneurons under DIC optics by the size and shape of their cell bodies, by visualization of somatic and dendritic morphology at the end of the recording session using Alexa Fluor dyes and epifluorescent illumination, and by post hoc visualization of intracellular Neurobiotin labeling using confocal methods (Figure 2B, Supplementary Figure 3A,B; n = 48 neurons from 9 mice). In a subset of experiments, we further characterized targeted cell types based on their intrinsic membrane properties, morphological features, and immunoreactivity for glutamate decarboxylase (GAD)

(Supplemental Figure 4). Across all auditory cortical layers and in both pyramidal neurons and inhibitory interneurons, brief (10 ms) illumination of SIn_{ACh} axon terminals near the recording site resulted in short latency, large amplitude and prolonged excitatory and inhibitory currents, which were measured at holding potentials of −70mV (EPSCs) and 0mV (IPSCs), respectively (Figure 2E,I; n = 28 neurons from 9 mice; EPSC: 72.67 ± 9.67 pA; IPSC: 82.43 ± 17.42 pA; Supplemental Figures 3C-E, 4). To further isolate postsynaptic nicotinic currents that SIn_{ACh} axon terminals evoke in auditory cortical pyramidal neurons and interneurons, we applied NBQX and AP5 to block glutamatergic transmission and atropine to block muscarinic ACh receptors. Under these conditions, optogenetic activation of SIn_{ACh} axon terminals still evoked prominent excitatory and inhibitory currents in both pyramidal neurons and interneurons (Figure 2F,I; Sn = 34 neurons from 6 mice; EPSC: 41.58 ± 4.12 pA; IPSC: 87.81 ± 16.22 pA; Supplemental Figure 4). These inhibitory currents lagged excitatory currents, and were abolished by bath application of Gabazine, indicating that they were mediated through $GABA_A$ receptors (Figure 2G,I-K; onset times: n = 12 neurons from 5 mice: EPSC: 10.41 ± 3.03 ms; IPSC: 27.58 ± 5.62 ms, p = 0.0085; Gabazine: n = 7 neurons from 4 mice; EPSC: 62.10 ± 13.04 pA; IPSC: 3.44 ± 0.41 pA). Remaining excitatory currents were abolished by the bath application of mecamylamine, a nicotinic ACh receptor antagonist (Figure 2H,I; p = 12 neurons from 8 mice; EPSC: 2.51 ± 0.274 pA; IPSC: 2.79 ± 0.56 pA). Thus SIn_{ACh} axons evoke excitatory and inhibitory currents across all auditory cortical layers and in different neuron types, and the excitatory currents can be largely attributed to fast nicotinic signaling onto both pyramidal neurons and inhibitory interneurons.

SIn_{ACh} axons depolarize ACtx neurons and modulate tone responses

The fast signaling mediated by SIn_{ACh} terminals in ACtx that we observed in brain slices raises the possibility that these cholinergic inputs can exert acute effects on auditory cortical neuron activity in vivo. To explore this possibility, we combined in vivo intracellular recordings from auditory cortical neurons with optogenetic stimulation of SIn_{ACh} axon terminals (Arroyo et al., 2012; Kalmbach et al., 2012). We expressed ChR2 in SIn_{ACh} axons using the same strategy described for brain slice experiments, then made sharp intracellular current clamp recordings from putative ACtx excitatory neurons (identified via online examination of intrinsic membrane properties and, in a small subset, subsequent morphological reconstruction) in urethane-anesthetized (n = 3) or awake, resting (n = 1) mice (Figure 3A, Supplemental Figure 5A). Illuminating the surface of ACtx around the recording site with blue light evoked small, sustained membrane depolarizations that persisted for several hundred milliseconds and that could be accompanied by an increase in spontaneous firing rate (Figure 3B-F; n = 11 cells; exemplar Vm: baseline: 1.729 ± 0.751 mV*s, laser: 7.104 ± 0.892 mV*s, $p = 4.89 \times 10^{-5}$; exemplar spike count: baseline: 5.03 ± 0.872 spikes, laser: 10.725 ± 0.518 spikes, $p = 1.44 \times 10^{-6}$; population Vm: baseline: 0.1799 ± 0.35 mV*s, laser: 2.033 ± 0.55 mV*s, p = 0.0048; Supplemental Figure 5B-E). To determine if these depolarizations modulated auditory cortical responses to sensory stimulation, we paired optogenetic stimulation (200 ms duration) of SIn_{ACh} axon terminals with tone pip presentation (50 ms duration, starting 100 ms after light onset). Such pairing resulted in a slight but significant enhancement of tone-evoked subthreshold membrane potential responses (Figure 3G, H, J, K; exemplar Vm: tone: 7.695 ± 1.021 mV*s, tone +

laser: 11.571 ± 0.765 mV*s, p = 0.002; population Vm: tone: 1.567 ± 0.76 mV*s, tone + laser: 2.959 ± 0.966 mV*s, p = 0.0176) and could also enhance action potential responses to tones (Figure 3I; exemplar spike count: tone: 13.8 ± 0.639 spikes, tone + laser: 15.5 ± 0.665 spikes, p = 0.015).

We used a multielectrode array to better assess how optogenetic stimulation of SIn_{ACh} axon terminals affected spiking activity as a function of tone responsiveness across larger populations of ACtx neurons (Figure 4A; n = 196 units from 5 urethane-anesthetized mice; spike sorting methods were used to measure single unit activity, and units were included for analysis if they responded significantly to sound presentation; units spanned a large area of cortex in both superficial and deep layers). We measured the effects of laser stimulation of SIn_{ACh} axon terminals on tone response strength (RS), which were on average facilitatory but quite mixed across the population (Figure 4B-E, Supplemental Figure F,G). To better understand this heterogeneity, we normalized tone RS and tone + laser RS of each unit to its peak tone RS, and aligned those values to produce population tuning curves with our without optogenetic stimulation of SIn_{ACh} axon terminals (Figure 4F)(Olsen et al., 2012). We then plotted normalized tone RS against normalized tone + laser RS, and fit a line to these points (Figure 4G). This analysis revealed that responses to non-preferred tones (those driving responses roughly 50% or less of peak tone response) were enhanced when those tones were paired with the laser. However, responses to the preferred tone (and to tones that evoked greater than 50% of peak tone response) were diminished with laser presentation. Thus, SIn_{ACh} stimulation results in a combination of additive and divisive modulation, reflected in the y-intercept of the linear regression (0.23), and the diminished slope of the regression (0.58). The net effect of SIn_{ACh} activation is to broaden the bandwidth of individual neurons while restricting the dynamic range of response strengths.

SIn_{ACh} axons in ACtx display elevated activity during movement

To address whether SIn_{ACh} axons convey movement-related signals to ACtx, we injected AAV-FLEX-GCaMP6s in SIn of ChAT-Cre mice, implanted a cranial window over ACtx, acclimated the mice to head fixation for several days, and then used two photon (2p) microscopy to image SIn_{ACh} axons in ACtx while simultaneously monitoring a variety of small body movements using a video camera and a treadmill rotary encoder (Figure 5A-D, Supplemental Figure 6A; we limited our analysis to small, non-locomotor movements that did not create z-axis artifacts when imaging small caliber SIn_{ACh} axons). Individual branches of SIn_{ACh} axons display elevated calcium levels across a range of body movements, including paw steps and mouth movements like whisking (Figure 5E-K; paw movements: n = 12 axons from 4 mice, baseline ΔF/F: −0.004 ± 0.008, moving ΔF/F: 0.051 ± 0.0159, p = 0.0063; mouth movements: n = 12 axons, baseline ΔF/F: 0.012 ± 0.0043, moving ΔF/F: 0.0495 ± 0.0124, p = 0.0022; all movements: n = 14 axons, baseline ΔF/F: 0.0132 ± 0.0041, moving ΔF/F: 0.0615 ± 0.0094, p = 7.04×10^{-5}).

The relationship between SIn_{ACh} axon activity in ACtx and other state-dependent signals

How is SIn_{ACh} axon activity related to other measures of brain state and to other movement-related signals that are transmitted to the ACtx? Prior studies have shown that microdilations of the pupil closely correlate with desynchronization of cortical membrane potential - a

neuronal state change that also accompanies movements (McGinley et al., 2015a; Reimer et al., 2014; Vinck et al., 2015). Therefore, we compared the timing of changes in SIn_{ACh} axon activity, measured with GCaMP6s to changes in pupil diameter (Figure 6A-C). We detected a peak correlation in SIn_{ACh} fluorescence that led pupil microdilations and followed movement onset by hundreds of milliseconds (Figure 6D-G; axons in example field of view, movements versus ΔF/F: 0.2652 ± 0.0227 s, ΔF/F versus pupil microdilations: 0.445 ± 0.0168 s; population data: movement versus ΔF/F: 0.3102 ± 0.0195 s; movement versus pupil: 0.8258 ± 0.1028 s). ACtx also receives information from a wide range of sources, including from premotor neurons located in the secondary motor cortex (M2) (Nelson et al., 2013; Schneider et al., 2014). We imaged M2 axon terminals in the ACtx and confirmed that they displayed heightened activity during a variety of movements. However, in contrast to the fairly uniform pattern of SIn_{ACh} axon activity during movement, M2 axons displayed a more temporally distributed pattern of activity, as has been observed in other sensory cortices (Supplemental Figure 6B-E)(Petreanu et al., 2012). Therefore, increases in SIn_{ACh} axon activity in the ACtx lead pupil microdilations, a feature associated with cortical membrane desynchronization, movement, and arousal, and are coactive with, yet qualitatively distinct from, movement-related activity of M2 axons.

Some auditory cortical neurons receive convergent input from SIn_{ACh} and M2 axons

The current findings that SIn_{ACh} axons are also active during movements raise the question of whether and how axon terminals from SIn_{ACh} and M2 neurons interact with each other in ACtx. We first used confocal microscopy to identify close appositions between SIn_{ACh} and M2 axons and ACtx neurons, which might reflect the presence of functionally convergent synapses. To map the distribution of SIn_{ACh} and M2 axon labeling across all ACtx layers, we injected AAV-FLEX-GFP into SIn and AAV-tdTomato into M2 of ChAT-Cre mice (Figure 7A-C). We then analyzed the distribution of labeled SIn_{ACh} and $M2_{ACtx}$ axons in ACtx, noting substantial overlap between these projections in all layers of ACtx (Figure 7D). Further, SIn_{ACh} and $M2_{ACtx}$ axons formed close appositions with cell bodies in ACtx, including those expressing nicotinic ACh receptors (Figure 7E-H, Supplemental Figure 7A-U). These structural features suggest that some auditory cortical neurons receive convergent synaptic input from both M2 and SIn_{ACh} neurons.

We used electrophysiological and optogenetic methods to directly test the possibility that single neurons receive synaptic input from M2 and SIn_{ACh} neurons. First, we injected AAV-FLEX-ChR2 into SIn and AAV-ChR2 into M2 of ChAT-Cre mice, resulting in ChR2 expression in both SIn_{ACh} and $M2_{ACtx}$ axon terminals (Figure 7I,J, Supplemental Figure 7V-Y). Whole-cell voltage clamp recordings from auditory cortical neurons in acute coronal brain slices revealed compound excitatory currents with fast and slow components following brief illumination at the recording site with blue light (Figure 7K; average trace of n = 5 neurons). A likely explanation is that these compound responses reflect the summation of fast glutamatergic currents evoked by $M2_{ACtx}$ axons and smaller yet more sustained cholinergic currents evoked by SIn_{ACh} axons. To test this idea, we bathed slices with NBQX, AP5, and atropine, thus eliminating fast glutamatergic $M2_{ACtx}$ currents as well as muscarinic currents. Under these conditions, residual currents closely resembled nicotinic ACh currents generated by stimulation of SIn_{ACh} axons alone (compare orange trace in

Figure 7K with Figure 2F, Supplemental Figure 7Z,AA). Measuring the time constants of evoked currents confirmed that the onset and offset kinetics slowed upon application of glutamate blockers, resulting in currents resembling those evoked from stimulation of SIn_{ACh} neurons alone (Figure 7L; τ_{on}, nACSF: 0.0038 ± 0.001 s, , τ_{on}, blockers: 0.086 ± 0.0198, p = 0.0138; τ_{off}, nACSF: 0.2412 ± 0.0155 s, τ_{off}, blockers: 0.4477 ± 0.0103 s, p = 3×10^{4}). Thus, SIn_{ACh} and $M2_{ACtx}$ axons provide convergent synaptic input to individual auditory cortical neurons.

SIn_{ACtx} and $M2_{ACtx}$ neurons receive distinct input from brainstem and forebrain regions

A remaining issue is whether SIn_{ACh} and M2 axons convey similar or different types of information to ACtx. One way of assessing this is to determine which brain regions provide synaptic input to the SIn and M2 neurons that project to the ACtx. We used an intersectional rabies-based trans-synaptic tracing approach to identify neurons that provide synaptic input to SIn_{ACtx} neurons. We injected AAV-FLEX-TVA-mCherry and AAV-FLEX-RG into SIn of wild-type mice followed by an injection of canine adenovirus expressing Cre (CAV-Cre) into ACtx (Figure 8A). Because CAV-Cre is retrogradely transported to cell bodies following infection via axons, this strategy results in recombination and expression of TVA-mCherry and RG in SIn_{ACtx} neurons. Following TVA/RG expression in SIn_{ACtx} neurons, EnVA-RΔG-GFP was injected into SIn, resulting in GFP expression in those neurons that make synapses on SIn_{ACtx} neurons (Figure 8A). First, we analyzed the local SIn microcircuit that provides input to SIn_{ACtx} neurons. We identified putative presynaptic SIn neurons (GFP+/mCherry-), finding that many of these neurons also were immunopositive for neuropeptide Y, injections of which into BF are correlated with changes in arousal and cortical EEG (Figure 8B-F) (Toth et al., 2007; Toth et al., 2005). We then identified several motor- or arousal-related brain regions outside of the SIn, primarily in the brainstem, that provide synaptic input to SIn_{ACtx} neurons. These included the cuneiform nucleus, the peripeduncular nucleus, periaqueductal gray, noradrenergic neurons in the locus coeruleus, serotonergic neurons in raphe, hypothalamus and frontal cortex (Figure 8G-O) (Arnault and Roger, 1987; Aston-Jones and Cohen, 2005; Jacobs and Fornal, 1993; Jürgens, 1994; Nelson et al., 2013; Saper et al., 2005; Shik et al., 1966). We then used a similar deficient rabies-based strategy to map neurons that provide synaptic input to $M2_{ACtx}$ neurons. In notable contrast to the inputs to SIn_{ACtx} neurons, $M2_{ACtx}$ neurons were targeted primarily by regions implicated in motor planning, decision-making and action initiation. These included motor thalamus, orbitofrontal cortex (segregated from OFC_{ACtx} projection neurons), retrosplenial cortex (RSD), somatosensory cortex, and rostral portions of BF (Supplemental Figure 8) (Mao et al., 2011; Prevosto and Sommer, 2013; Vann et al., 2009; Wallis, 2007). These findings support the idea that SIn_{ACtx} neurons receive input from motor- and state-related brain regions, and that many of their inputs are distinct from $M2_{ACtx}$ neurons. Therefore, SIn_{ACtx} and $M2_{ACtx}$ neurons both transmit movement-related signals to ACtx, but with different temporal profiles and presumably conveying different types of movement-related information.

Discussion

The current study establishes that cholinergic axon terminals in the auditory cortex provide fast movement-related signals that operate in close spatiotemporal parallel with movement-related signals from the motor cortex. These cholinergic inputs arise from the caudal part of the basal forebrain (i.e., SIn) and receive input from brainstem regions implicated in movement and arousal, whereas motor cortical neurons that innervate ACtx receive information mostly from forebrain regions, including those implicated in motor planning. SIn cholinergic axons synapse on a variety of inhibitory and excitatory cell types across all auditory cortical layers, and single auditory cortical neurons can receive input from both cholinergic and motor cortical afferents, providing cellular loci where modulatory signals important to learning and arousal can influence rapid movement-related signals from the motor cortex. Thus, cholinergic inputs are well suited to contribute to fast, movement-related modulation of auditory cortical processing and to a more gradual modification of auditory cortical response properties, including the learning of new motor-auditory associations.

The cholinergic cells that provide synaptic input to ACtx are a dispersed population of magnocellular neurons located in the caudal BF (i.e., SIn). Their anatomical location agrees with previous efforts to study the influence of BF on ACtx in rodents using electrical stimulation (Bakin and Weinberger, 1996; Froemke et al., 2013). However, the intersectional genetic methods used here allowed us to isolate the specific contribution of cholinergic projections to different auditory cortical cell types, without the confound of recruiting neighboring noncholinergic cell bodies or axons of passage, which can occur with electrical stimulation (Lin et al., 2006). Moreover, the presynaptic tracing methods used here benefit from the specific spread of rabies virus through functional synapses and not through closely juxtaposed non-synaptic axonal processes (Callaway, 2008; Ekstrand et al., 2008; Ugolini, 1995, 2008; Wickersham et al., 2007a; Wickersham et al., 2007b). The benefits of this synaptic specificity – along with previous ultrastructural characterization of cholinergic varicosities – leads us to conclude that a significant portion of cholinergic transmission in ACtx is mediated synaptically (Smiley et al., 1997; Takacs et al., 2013; Turrini et al., 2001). This does not discount the possibility of extrasynaptic cholinergic signalling, which may act alongside synaptic signaling mechanisms to modulate auditory cortical activity, particularly on slower timescales. Nevertheless, optogenetic stimulation of SIn_{ACh} axon terminals in vitro and in vivo evokes fast excitatory and inhibitory synaptic currents in ACtx, rather than driving only a slow modulatory signal.

A combination of in vivo electrophysiological and optogenetic methods reveal that the net effect of SIn_{ACh} stimulation is to facilitate weak auditory cortical responses and suppress stronger responses, effectively broadening the response bandwidth. These data confirm and extend previous studies that injected cholinergic agonists into ACtx by revealing that endogenous cholinergic release exerts rapid functional effects of on auditory cortical responses (McKenna et al., 1988; McKenna et al., 1989; Metherate et al., 1990). The ability of SIn_{ACh} axons to rapidly modulate auditory cortical responses points to a mechanism involving postsynaptic nicotinic receptors. However, in the intact brain, SIn_{ACh} axons may modulate auditory cortical neuron activity through additional pathways, including muscarinic receptors, presynaptic cholinergic receptors, and the co-release of other

neurotransmitters, such as GABA, as well as through polysynaptic mechanisms (Disney et al., 2007; Gil et al., 1997; Kim et al., 2015; Lin et al., 2015; Lin et al., 2006; Pi et al., 2013; Saunders et al., 2015). In fact, our failure to observe excitatory currents mediated by nicotinic receptors in fast spiking (FS) neurons is consistent with evidence that cholinergic signaling modulates this cell type indirectly through other inhibitory interneurons (Chen et al., 2015; Fu et al., 2014). Nonetheless, the present finding that SIn_{ACh} axons directly excite inhibitory and excitatory interneurons, as well as pyramidal neurons through postsynaptic nicotinic receptors suggests activation of these ionotropic receptors is sufficient to account for rapid facilitation and suppression of auditory cortical responses. The fast actions of SIn_{ACh} axons make them well suited for the rapid modulation of auditory cortical receptive fields during behavioral tasks requiring attention, a process that is hypothesized to be heavily influenced by cholinergic signaling (DeWeese et al., 2005; Fritz et al., 2003; Hocherman et al., 1976), and for coinciding with fast movement-related signals from motor cortical regions.

An unresolved issue is how cholinergic transmission can facilitate or suppress cortical responses to tones as a function of response strength. One possibility is that cholinergic activity amplifies recurrent inhibition in ACtx elicited by strong thalamocortical activity, suppressing responses to preferred tones. In contrast, cholinergic activity in the presence of weaker thalamocortical activity may be insufficient to recruit inhibitory networks, resulting in facilitation. Prior studies show that acetylcholine can directly excite a variety of cortical interneurons, including SST^+, VIP^+, and possibly PV^+ cells (Arroyo et al., 2012; Christophe et al., 2002; Fanselow et al., 2008; Gulledge et al., 2007; Kawaguchi, 1997; Krenz et al., 2001; Kruglikov and Rudy, 2008; Nunez et al., 2012; Poorthuis et al., 2013; Yamamoto et al., 2010). The current findings extend these earlier observations by showing that SIn_{ACh} axons can excite excitatory and inhibitory neurons in ACtx, providing a substrate for both facilitating and suppressing auditory responsiveness.

While recent efforts have helped to characterize how cholinergic projections to sensory cortex are active across different behaviors, a characterization of their movement-related activity patterns in the auditory cortex was lacking (Eggermann et al., 2014; Hangya et al., 2015; Lin et al., 2015). In vivo 2p imaging experiments revealed that SIn_{ACh} axons are active during a range of body movements, including small, non-locomotor movements like whisking, licking, and paw steps. While we focused on these movements to limit motion-induced artifacts, substantial changes in membrane potential activity in ACtx neurons accompany slight movements, indicating that focusing on these small movements is relevant to auditory cortical processing (Schneider and Mooney, 2015; Schneider et al., 2014). Importantly, both SIn_{ACh} activity and movements preceded pupil microdilations, which are known to track changes in cortical state (McGinley et al., 2015a; Reimer et al., 2014; Vinck et al., 2015). In fact, common circuitry is speculated to drive both pupil microdilations and changes in cortical state, both of which at times may occur independently of locomotion (McGinley et al., 2015b). Indeed, because microdilations followed SIn_{ACh} activity, it is plausible that neuromodulatory circuits including the BF could be involved in driving changes in pupil diameter. However, we found that pupil microdilations frequently followed smaller movements that were independent of locomotion and otherwise undetectable by monitoring treadmill rotation alone. Therefore, another possibility is that neurons important

to motor planning, including $M2_{ACtx}$ neurons, drive pupillary changes and a variety of other movements in parallel.

Although SIn_{ACh} and M2 axons in ACtx both display movement-related activity, $M2_{ACtx}$ and SIn_{ACtx} neurons receive input from distinct brain regions, suggesting that they convey distinct types of information. Specifically, intersectional tracing methods show that $M2_{ACtx}$ neurons receive input from a variety of cortical regions implicated in motor planning, such as OFC and RSD (Vann et al., 2009; Wallis, 2007). Together, this pattern of connectivity supports the notion that this pathway contributes to top-down information transmission, informing auditory cortical neurons of impending decisions concerning body movements and other behaviors (Crapse and Sommer, 2008; Schneider and Mooney, 2015). In contrast to $M2_{ACtx}$ neurons, SIn_{ACtx} neurons receive input predominantly from brainstem regions thought to be more intimately related to movement generation and states of arousal, including the cuneiform nucleus, a component of the mesencephalic locomotor region (Lee et al., 2014; Roseberry et al., 2016; Shik et al., 1966). Additionally, we found that SIn_{ACtx} neurons are targeted by other neuromodulatory projections from LC and raphe, as well as local NPY SIn interneurons, which are known to regulate the activity of cholinergic projection neurons, and in turn control changes in arousal and cortical activity (Aston-Jones and Cohen, 2005; Toth et al., 2007; Toth et al., 2005). Finally, SIn_{ACtx} neurons are targeted by neurons in PAG and a dispersed population in the hypothalamus, which could enable them to relay information about arousal and reproductive state to ACtx (Burgdorf et al., 2007; Jürgens, 1994; Oliveras et al., 1974; Saper et al., 2005; Storozhuk et al., 1984). This convergent architecture enables the auditory cortex to integrate bottom-up neuromodulatory signals related to ongoing movements and internal state with top-down information concerning impending movements and motor planning.

Experimental Procedures

Animal Preparation and Stereotaxic Injections

All experimental protocols were approved by Duke University Institutional Animal Care and Use Committee. Male and female mice were purchased from Jackson Laboratories and housed and bred in an onsite vivarium. Mice selected for surgical and experimental procedures were kept on a reverse light cycle. Mice aged 1-2 months (for in vitro electrophysiology) or 2-4 months (all other injections) were anesthetized with isoflurane (1-2% in O_2) and placed in a stereotaxic apparatus. Viruses were pressure injected into the brain region of interest, and mice were allowed to recover for 14 days, or 7 days following injections of rabies virus. See Supplemental Experimental Procedures for additional information.

Slice Electrophysiology

Whole-cell recordings were made from acute coronal brain slices, using patch electrodes (2–6 M) filled with an internal solution of 5 mM QX-314, 2 mM ATP Mg salt, 0.3 mM GTP Na salt, 10 mM phosphocreatine, 0.2 mM EGTA, 2 mM $MgCl_2$, 5 mM NaCl, 10 mM HEPES, 120 mM cesium methanesulfonate, 0.15% Neurobiotin, and 0.1 mM Alexa Fluor 594 cadaverine or 0.1 mM Alexa Fluor 488 Na salt. Series resistance was always < 25 MΩ

and was compensated up to 90%. See Supplemental Experimental Procedures for additional information.

In Vivo Electrophysiology

One to 7 days before physiology, mice were anesthetized with isoflurane and a custom titanium plate was attached to the skull with Metabond (Parkell), leaving ACtx exposed. For recording from awake mice, animals were acclimated to head fixation for several days. For intracellular recordings, a small craniotomy was made over ACtx, and a sharp glass electrode was lowered into the brain until the tip penetrated a neuron. Neurons were used for further analysis only if the resting membrane potential was less than −50 mV and was modulated by an auditory stimulus. For extracellular recordings, a 32-channel multielectrode array (NeuroNexus) was lowered into ACtx. Putative action potentials were identified by voltage events crossing a threshold, and individual neurons were sorted based on spike features using custom software. See Supplemental Experimental Procedures for additional information.

2 Photon Calcium Imaging

Three to four weeks following the GCaMP6s injection, mice were anaesthetized with isoflurane and a custom, Y-shaped titanium plate was attached to the skull with Metabond. Mice were acclimated to head fixation for 1–5 days. A rectangular craniotomy was then made over the injection site, and a laminated glass coverslip was placed over the craniotomy and sealed with Metabond. Imaging was performed using a resonant scanning two-photon microscope (Neurolabware) with a mode-locked titanium sapphire laser (Mai Tai DeepSee) at 920 nm. A small infrared-sensitive video camera (Logitech) was positioned to monitor body movements. A GigE Vision camera (Dalsa) was used to monitor changes in pupil size at an acquisition rate synchronized to that of the microscope. Regions of interest (ROIs) were selected either by manually tracing around short, independent segments of axon, or by using semi-automated identification of nearby correlated pixel activity (Scanbox). See Supplemental Experimental Procedures for additional information.

Movement Tracking and Pupillometry

Body movements were detected offline using ROIs drawn around the head (including mouth, nose, and whiskers), forelimbs, and treadmill perimeter, as well as a red LED used to synchronize video and 2p data. Pupil size was similarly quantified by measuring the change in average pixel intensity within an ROI drawn around the eye. Pupil area traces were low-pass filtered to remove movement artifacts, which were clearly distinguishable from both slow and fast pupil dilations and constrictions.

Histology and Confocal Microscopy

Immunostaining was performed with primary antibodies in PBST with 10% Blocking One blocking buffer (Nacalai Tesque) for 2-3 nights at 4°C. After three washes of 10 min in PBS, slices were incubated in secondary antibodies from Jackson Immunoresearch at a concentration of 1:1000 in PBST containing 10% blocking buffer overnight at 4°C. Images were acquired with a Zeiss 710 LSM inverted confocal microscope using 10x, 20x, 60x oil

immersion, or 100x oil immersion objectives. For presentation, some images were median filtered with a window radius of one pixel. Additionally, a subset of Z stacks underwent 3D interpolation with a resampling factor of one (3D Viewer, Image J) to permit rotated views of images. See Supplemental Experimental Procedures for additional information.

Data Analysis

All data analyses were performed in Matlab. For all statistical tests, significance was measured against an alpha of 0.05. See Supplemental Experimental Procedures for additional information.

Supplementary Material

Refer to Web version on PubMed Central for supplementary material.

Acknowledgements

We thank Dr. David Schneider for help with data analysis and experiments using extracellular multielectrode recordings. We thank Drs. Ben Philpot, Dale Purves, David Schneider, Katherine Tschida, and Fan Wang for comments on the manuscript. This research was supported by the Holland-Trice Graduate Fellowship in Brain Science, and NIH grants 1R01-DC013826-01A1 to R.M. and 1 F31 DC013976-01 to A.N.

References

Arnault P, Roger M. The connections of the peripeduncular area studied by retrograde and anterograde transport in the rat. The Journal of Comparative Neurology. 1987; 258:463–476. [PubMed: 3584548]

Arroyo S, Bennett C, Aziz D, Brown S, Hestrin S. Prolonged disynaptic inhibition in the cortex mediated by slow, non-α7 nicotinic excitation of a specific subset of cortical interneurons. The Journal of neuroscience. 2012; 32:3859–3864. [PubMed: 22423106]

Aston-Jones G, Cohen JD. An integrative theory of locus coeruleusnorepinephrine function: adaptive gain and optimal performance. Annual Review of Neuroscience. 2005; 28:403–450.

Bakin JS, Weinberger NM. Induction of a physiological memory in the cerebral cortex by stimulation of the nucleus basalis. Proceedings of the National Academy of Sciences of the United States of America. 1996; 93:11219–11224. [PubMed: 8855336]

Budinger E, Laszcz A, Lison H, Scheich H, Ohl F. Non-sensory cortical and subcortical connections of the primary auditory cortex in Mongolian gerbils: bottom-up and top-down processing of neuronal information via field AI. Brain Research. 2008; 1220:2–32. [PubMed: 17964556]

Burgdorf J, Wood P, Kroes R, Moskal J, Panksepp J. Neurobiology of 50-kHz ultrasonic vocalizations in rats: electrode mapping, lesion, and pharmacology studies. Behav Brain Res. 2007; 182:274–283. [PubMed: 17449117]

Callaway EM. Transneuronal circuit tracing with neurotropic viruses. Current Opinion in Neurobiology. 2008; 18:617–623. [PubMed: 19349161]

Chen N, Sugihara H, Sur M. An acetylcholine-activated microcircuit drives temporal dynamics of cortical activity. Nature Neuroscience. 2015; 18:892–902. [PubMed: 25915477]

Christophe E, Roebuck A, Staiger JF, Lavery DJ, Charpak S, Audinat E. Two types of nicotinic receptors mediate an excitation of neocortical layer I interneurons. Journal of Neurophysiology. 2002; 88:1318–1327. [PubMed: 12205153]

Crapse T, Sommer M. Corollary discharge across the animal kingdom. Nature reviews Neuroscience. 2008; 9:587–600. [PubMed: 18641666]

DeWeese MR, Hromadka T, Zador AM. Reliability and representational bandwidth in the auditory cortex. Neuron. 2005; 48:479–488. [PubMed: 16269364]

Disney AA, Aoki C, Hawken MJ. Gain modulation by nicotine in macaque V1. Neuron. 2007; 56:701–713. [PubMed: 18031686]

Eggermann E, Kremer Y, Crochet S, Petersen CC. Cholinergic signals in mouse barrel cortex during active whisker sensing. Cell Reports. 2014; 9:1654–1660. [PubMed: 25482555]

Ekstrand MI, Enquist LW, Pomeranz LE. The alpha-herpesviruses: molecular pathfinders in nervous system circuits. Trends Mol Med. 2008; 14:134–140. [PubMed: 18280208]

Eliades S, Wang X. Sensory-motor interaction in the primate auditory cortex during self-initiated vocalizations. Journal of Neurophysiology. 2003; 89:2194–2207. [PubMed: 12612021]

Everitt BJ, Robbins TW. Central cholinergic systems and cognition. Annual Review of Psychology. 1997; 48:649–684.

Fanselow EE, Richardson KA, Connors BW. Selective, State-Dependent Activation of Somatostatin-Expressing Inhibitory Interneurons in Mouse Neocortex. Journal of Neurophysiology. 2008; 100:2640–2652. [PubMed: 18799598]

Fritz J, Shamma S, Elhilali M, Klein D. Rapid task-related plasticity of spectrotemporal receptive fields in primary auditory cortex. Nature Neuroscience. 2003; 6:1216–1223. [PubMed: 14583754]

Froemke R, Merzenich M, Schreiner C. A synaptic memory trace for cortical receptive field plasticity. Nature. 2007; 450:425–429. [PubMed: 18004384]

Froemke RC, Carcea I, Barker AJ, Yuan K, Seybold BA, Martins AR, Zaika N, Bernstein H, Wachs M, Levis PA, et al. Long-term modification of cortical synapses improves sensory perception. Nature Neuroscience. 2013; 16:79–88. [PubMed: 23178974]

Fu Y, Tucciarone JM, Espinosa JS, Sheng N, Darcy DP, Nicoll RA, Huang ZJ, Stryker MP. A cortical circuit for gain control by behavioral state. Cell. 2014; 156:1139–1152. [PubMed: 24630718]

Gil Z, Connors BW, Amitai Y. Differential regulation of neocortical synapses by neuromodulators and activity. Neuron. 1997; 19:679–686. [PubMed: 9331357]

Gulledge AT, Park SB, Kawaguchi Y, Stuart GJ. Heterogeneity of phasic cholinergic signaling in neocortical neurons. Journal of Neurophysiology. 2007; 97:2215–2229. [PubMed: 17122323]

Hangya B, Ranade SP, Lorenc M, Kepecs A. Central Cholinergic Neurons Are Rapidly Recruited by Reinforcement Feedback. Cell. 2015; 162:1155–1168. [PubMed: 26317475]

Hedrick T, Waters J. Physiological properties of cholinergic and non-cholinergic magnocellular neurons in acute slices from adult mouse nucleus basalis. PloS One. 2010; 5:e11046. [PubMed: 20548784]

Hocherman S, Benson DA, Goldstein MH Jr. Heffner HE, Hienz RD. Evoked unit activity in auditory cortex of monkeys performing a selective attention task. Brain research. 1976; 117:51–68. [PubMed: 825193]

Jacobs BL, Fornal CA. 5-HT and motor control: a hypothesis. Trends in Neurosciences. 1993; 16:346–352. [PubMed: 7694403]

Johnston MV, McKinney M, Coyle JT. Neocortical cholinergic innervation: a description of extrinsic and intrinsic components in the rat. Exp Brain Res. 1981; 43:159–172. [PubMed: 6265265]

Jürgens U. The role of the periaqueductal grey in vocal behaviour. Behav Brain Res. 1994; 62:107–117. [PubMed: 7945960]

Kalmbach A, Hedrick T, Waters J. Selective optogenetic stimulation of cholinergic axons in neocortex. Journal of Neurophysiology. 2012; 107:2008–2019. [PubMed: 22236708]

Kawaguchi Y. Selective cholinergic modulation of cortical GABAergic cell subtypes. Journal of Neurophysiology. 1997; 78:1743–1747. [PubMed: 9310461]

Kilgard M, Merzenich M. Cortical map reorganization enabled by nucleus basalis activity. Science. 1998; 279:1714–1718. [PubMed: 9497289]

Kim T, Thankachan S, McKenna JT, McNally JM, Yang C, Choi JH, Chen L, Kocsis B, Deisseroth K, Strecker RE, et al. Cortically projecting basal forebrain parvalbumin neurons regulate cortical gamma band oscillations. Proceedings of the National Academy of Sciences of the United States of America. 2015; 112:3535–3540. [PubMed: 25733878]

Krenz I, Kalkan D, Wevers A, de Vos RA, Steur EN, Lindstrom J, Pilz K, Nowacki S, Schutz U, Moser N, et al. Parvalbumin-containing interneurons of the human cerebral cortex express nicotinic acetylcholine receptor proteins. J Chem Neuroanat. 2001; 21:239–246. [PubMed: 11382535]

Kruglikov I, Rudy B. Perisomatic GABA release and thalamocortical integration onto neocortical excitatory cells are regulated by neuromodulators. Neuron. 2008; 58:911–924. [PubMed: 18579081]

Lee AM, Hoy JL, Bonci A, Wilbrecht L, Stryker MP, Niell CM. Identification of a Brainstem Circuit Regulating Visual Cortical State in Parallel with Locomotion. Neuron. 2014; 83:455–466. [PubMed: 25033185]

Letzkus J, Wolff S, Meyer EM, Tovote P, Courtin J, Herry C, Lüthi A. A disinhibitory microcircuit for associative fear learning in the auditory cortex. Nature. 2011; 480:331–335. [PubMed: 22158104]

Lin SC, Brown RE, Hussain Shuler MG, Petersen CC, Kepecs A. Optogenetic Dissection of the Basal Forebrain Neuromodulatory Control of Cortical Activation, Plasticity, and Cognition. The Journal of Neuroscience. 2015; 35:13896–13903. [PubMed: 26468190]

Lin SC, Gervasoni D, Nicolelis MA. Fast modulation of prefrontal cortex activity by basal forebrain noncholinergic neuronal ensembles. Journal of Neurophysiology. 2006; 96:3209–3219. [PubMed: 16928796]

Mao T, Kusefoglu D, Hooks B, Huber D, Petreanu L, Svoboda K. Long-range neuronal circuits underlying the interaction between sensory and motor cortex. Neuron. 2011; 72:111–123. [PubMed: 21982373]

McGinley MJ, David SV, McCormick DA. Cortical Membrane Potential Signature of Optimal States for Sensory Signal Detection. Neuron. 2015a; 87:179–192. [PubMed: 26074005]

McGinley MJ, Vinck M, Reimer J, Batista-Brito R, Zagha E, Cadwell CR, Tolias AS, Cardin JA, McCormick DA. Waking State: Rapid Variations Modulate Neural and Behavioral Responses. Neuron. 2015b; 87:1143–1161. [PubMed: 26402600]

McKenna TM, Ashe JH, Hui GK, Weinberger NM. Muscarinic agonists modulate spontaneous and evoked unit discharge in auditory cortex of cat. Synapse. 1988; 2:54–68. [PubMed: 3420531]

McKenna TM, Ashe JH, Weinberger NM. Cholinergic modulation of frequency receptive fields in auditory cortex: I. Frequency-specific effects of muscarinic agonists. Synapse. 1989; 4:30–43. [PubMed: 2672402]

Metherate R, Ashe JH, Weinberger NM. Acetylcholine modifies neuronal acoustic rate-level functions in guinea pig auditory cortex by an action at muscarinic receptors. Synapse. 1990; 6:364–368. [PubMed: 2287993]

Metherate R, Cox CL, Ashe JH. Cellular bases of neocortical activation: modulation of neural oscillations by the nucleus basalis and endogenous acetylcholine. The Journal of Neuroscience. 1992; 12:4701–4711. [PubMed: 1361197]

Munoz W, Rudy B. Spatiotemporal specificity in cholinergic control of neocortical function. Current Opinion in Neurobiology. 2014; 26:149–160. [PubMed: 24637201]

Nelson A, Schneider DM, Takatoh J, Sakurai K, Wang F, Mooney R. A circuit for motor cortical modulation of auditory cortical activity. The Journal of Neuroscience. 2013; 33:14342–14353. [PubMed: 24005287]

Nunez A, Dominguez S, Buno W, Fernandez de Sevilla D. Cholinergic-mediated response enhancement in barrel cortex layer V pyramidal neurons. Journal of Neurophysiology. 2012; 108:1656–1668. [PubMed: 22723675]

Oliveras JL, Woda A, Guilbaud G, Besson JM. Inhibition of the jaw opening reflex by electrical stimulation of the periaqueductal gray matter in the awake, unrestrained cat. Brain Research. 1974; 72:328–331. [PubMed: 4838384]

Olsen SR, Bortone DS, Adesnik H, Scanziani M. Gain control by layer six in cortical circuits of vision. Nature. 2012; 483:47–U83. [PubMed: 22367547]

Petreanu L, Gutnisky DA, Huber D, Xu NL, O'Connor DH, Tian L, Looger L, Svoboda K. Activity in motor-sensory projections reveals distributed coding in somatosensation. Nature. 2012; 489:299–303. [PubMed: 22922646]

Pi HJ, Hangya B, Kvitsiani D, Sanders JI, Huang ZJ, Kepecs A. Cortical interneurons that specialize in disinhibitory control. Nature. 2013; 503:521. [PubMed: 24097352]

Pinto L, Goard MJ, Estandian D, Xu M, Kwan AC, Lee SH, Harrison TC, Feng G, Dan Y. Fast modulation of visual perception by basal forebrain cholinergic neurons. Nature Neuroscience. 2013; 16:1857–1863. [PubMed: 24162654]

Polley D, Steinberg E, Merzenich M. Perceptual learning directs auditory cortical map reorganization through top-down influences. The Journal of Neuroscience. 2006; 26:4970–4982. [PubMed: 16672673]

Poorthuis RB, Bloem B, Schak B, Wester J, de Kock CPJ, Mansvelder HD. Layer-Specific Modulation of the Prefrontal Cortex by Nicotinic Acetylcholine Receptors. Cerebral Cortex. 2013; 23:148–161. [PubMed: 22291029]

Prevosto V, Sommer MA. Cognitive control of movement via the cerebellar-recipient thalamus. Front Syst Neurosci. 2013; 7:56. [PubMed: 24101896]

Reimer J, Froudarakis E, Cadwell CR, Yatsenko D, Denfield GH, Tolias AS. Pupil fluctuations track fast switching of cortical states during quiet wakefulness. Neuron. 2014; 84:355–362. [PubMed: 25374359]

Roseberry TK, Lee AM, Lalive AL, Wilbrecht L, Bonci A, Kreitzer AC. Cell-Type-Specific Control of Brainstem Locomotor Circuits by Basal Ganglia. Cell. 2016; 164:526–537. [PubMed: 26824660]

Saper CB, Scammell TE, Lu J. Hypothalamic regulation of sleep and circadian rhythms. Nature. 2005; 437:1257–1263. [PubMed: 16251950]

Sarter M, Hasselmo ME, Bruno JP, Givens B. Unraveling the attentional functions of cortical cholinergic inputs: interactions between signal-driven and cognitive modulation of signal detection. Brain Research Brain Research Reviews. 2005; 48:98–111. [PubMed: 15708630]

Saunders A, Granger AJ, Sabatini BL. Corelease of acetylcholine and GABA from cholinergic forebrain neurons. eLife. 2015; 4

Schneider DM, Mooney R. Motor-related signals in the auditory system for listening and learning. Current Opinion in Neurobiology. 2015; 33:78–84. [PubMed: 25827273]

Schneider DM, Nelson A, Mooney R. A synaptic and circuit basis for corollary discharge in the auditory cortex. Nature. 2014; 513:189–194. [PubMed: 25162524]

Shik ML, Severin FV, Orlovskii GN. Control of walking and running by means of electric stimulation of the midbrain. Biofizika. 1966; 11:659–666. [PubMed: 6000625]

Smiley JF, Morrell F, Mesulam MM. Cholinergic synapses in human cerebral cortex: an ultrastructural study in serial sections. Experimental Neurology. 1997; 144:361–368. [PubMed: 9168836]

Storozhuk VM, Ivanova SF, Talnov AN. Role of the Midbrain Periaqueductal Gray-Matter in Conditioned Reflexes. Neurophysiology. 1984; 16:320–332.

Takacs VT, Freund TF, Nyiri G. Neuroligin 2 Is Expressed in Synapses Established by Cholinergic Cells in the Mouse Brain. PloS one. 2013; 8

Toth A, Hajnik T, Zaborszky L, Detari L. Effect of basal forebrain neuropeptide Y administration on sleep and spontaneous behavior in freely moving rats. Brain Research Bulletin. 2007; 72:293–301. [PubMed: 17452289]

Toth A, Zaborszky L, Detari L. EEG effect of basal forebrain neuropeptide Y administration in urethane anaesthetized rats. Brain Research Bulletin. 2005; 66:37–42. [PubMed: 15925142]

Turrini P, Casu MA, Wong TP, De Koninck Y, Ribeiro-Da-Silva A, Cuello AC. Cholinergic nerve terminals establish classical synapses in the rat cerebral cortex: Synaptic pattern and age-related atrophy. Neuroscience. 2001; 105:277–285. [PubMed: 11672595]

Ugolini G. Specificity of Rabies Virus as a Transneuronal Tracer of Motor Networks -Transfer from Hypoglossal Motoneurons to Connected 2nd-Order and Higher-Order Central-Nervous-System Cell Groups. Journal of Comparative Neurology. 1995; 356:457–480. [PubMed: 7642806]

Ugolini G. Use of rabies virus as a transneuronal tracer of neuronal connections: Implications for the understanding of rabies pathogenesis. Dev Biologicals. 2008; 131:493–506.

Unal CT, Golowasch JP, Zaborszky L. Adult mouse basal forebrain harbors two distinct cholinergic populations defined by their electrophysiology. Frontiers in Behavioral Neuroscience. 2012; 6:21. [PubMed: 22586380]

Vann SD, Aggleton JP, Maguire EA. What does the retrosplenial cortex do? Nature Reviews Neuroscience. 2009; 10:792–U750. [PubMed: 19812579]

Vinck M, Batista-Brito R, Knoblich U, Cardin JA. Arousal and Locomotion Make Distinct Contributions to Cortical Activity Patterns and Visual Encoding. Neuron. 2015; 86:740–754. [PubMed: 25892300]

Wallis JD. Orbitofrontal cortex and its contribution to decision-making. Annual Review of Neuroscience. 2007; 30:31–56.

Wickersham I, Finke S, Conzelmann K-K, Callaway E. Retrograde neuronal tracing with a deletion-mutant rabies virus. Nature Methods. 2007a; 4:47–49. [PubMed: 17179932]

Wickersham I, Lyon D, Barnard R, Mori T, Finke S, Conzelmann K-K, Young J, Callaway E. Monosynaptic restriction of transsynaptic tracing from single, genetically targeted neurons. Neuron. 2007b; 53:639–647. [PubMed: 17329205]

Yamamoto K, Koyanagi Y, Koshikawa N, Kobayashi M. Postsynaptic Cell Type-Dependent Cholinergic Regulation of GABAergic Synaptic Transmission in Rat Insular Cortex. Journal of Neurophysiology. 2010; 104:1933–1945. [PubMed: 20685921]

Zaborszky L, Duque A. Local synaptic connections of basal forebrain neurons. Behav Brain Res. 2000; 115:143–158. [PubMed: 11000417]

Zaborszky L, Pang K, Somogyi J, Nadasdy Z, Kallo I. The basal forebrain corticopetal system revisited. Annals of the New York Academy of Sciences. 1999; 877:339–367. [PubMed: 10415658]

Highlights

- Cholinergic basal forebrain (BF) neurons target several auditory cortical cell types
- Stimulation of cholinergic BF axons broadens auditory cortical responsiveness
- Cholinergic BF axons are active during body movements and before pupil microdilations
- Motor cortex and BF synapse on single neurons, but convey distinct information

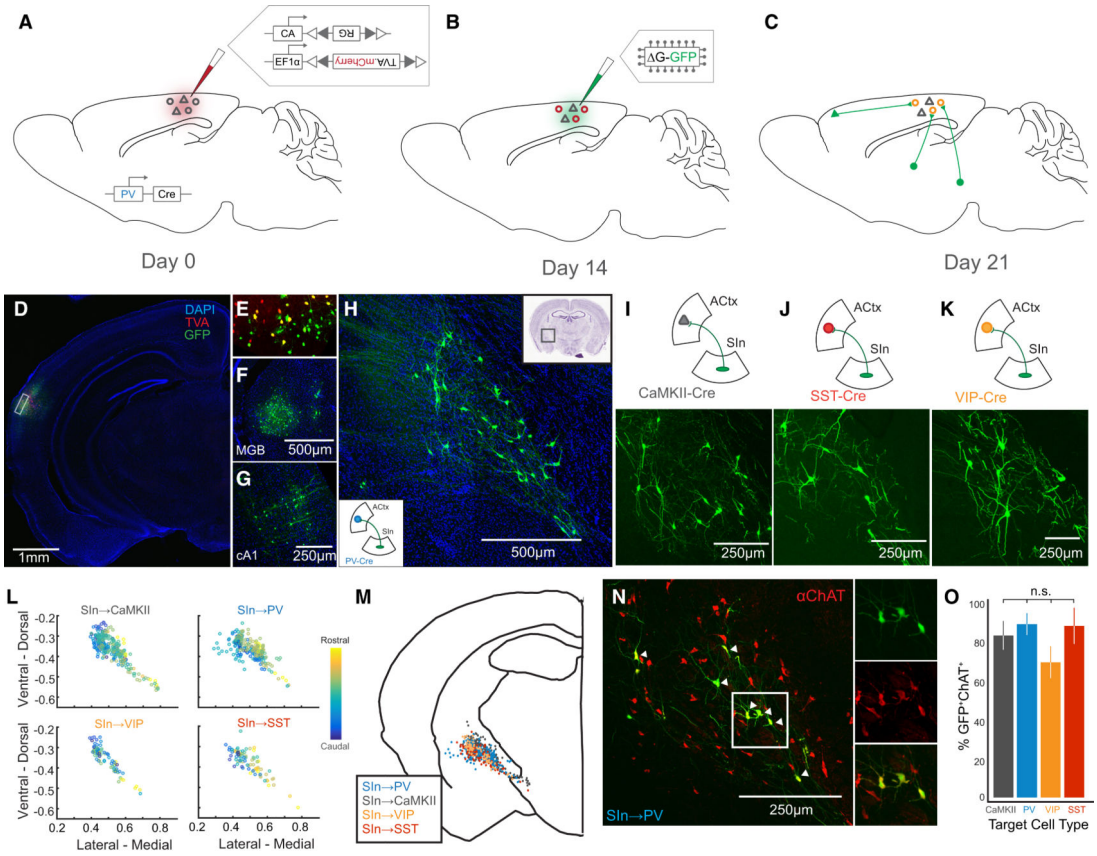

Figure 1. Cholinergic SIn Neurons Target the Major Cell Types of ACtx

(A-C) Overview of the rabies-based monosynaptic, presynaptic tracing strategy. (A) On day 0, AAV-FLEX-RG and AAV-FLEX-TVA.mCherry were injected into ACtx of a Cre driver mouse, in this case PV-Cre. (B) On day 14, EnVA-RΔG.GFP was injected into ACtx, which labeled neurons presynaptic to PV cells expressing TVA and RG (C). (D) GFP and mCherry labeling in ACtx. (E) Inset from (D) showing GFP^+, $mCherry^+$, and double-labeled neurons. (F) GFP^+ neurons (presynaptic to PV neurons in ACtx) in MGB. (G) GFP^+ neurons in contralateral ACtx. (H) GFP^+ neurons in SIn. The lower left inset diagrams the target of SIn neurons for this experiment. The upper right inset indicates the location of SIn_{ACtx} labeling on a coronal brain slice (from Paxinos & Franklin). (I-K) Top panels indicate the location and target cell type of the GFP^+ labeling in lower panels. (L) The coronal brain coordinates for SIn_{ACtx} neurons presynaptic to four cell types of ACtx, relative to a common midline landmark and normalized by brain slice size (n = 2 mice for each plot). The color code indicates rostral-caudal location of labeled neurons. (M) Locations of SIn neurons targeting different ACtx cell types superimposed on a generalized coronal brain slice (n = 8 mice total). (N) ChAT immunolabeling in GFP+ SIn neurons targeting PV^+ ACtx neurons. Double-labeled SIn_{ACtx} neurons (SIn_{ACh} neurons are indicated with arrowheads). Panels to the right show GFP^+ neurons (top), $ChAT^+$ neurons (middle), and overlaid images (bottom). (O) Percent $ChAT^+GFP^+$ SIn neurons for each target ACtx cell type (CaMKII, n = 3; PV, n = 2; VIP, n = 3; SST, n = 3). (n.s. $p > 0.05$). Values are mean ± SEM.

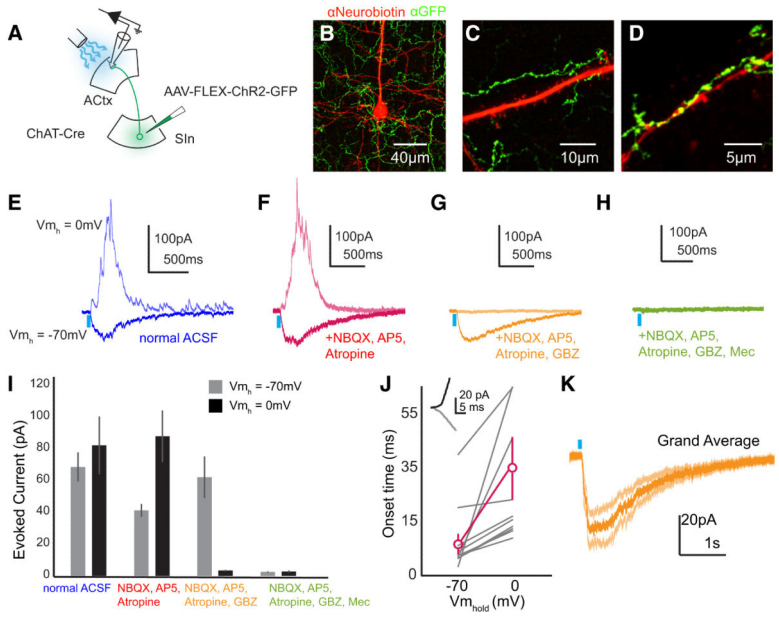

Figure 2. SIn_{ACh} Neurons evoke excitatory and inhibitory currents in ACtx neurons

(A) Schematic of the experimental strategy. AAV-FLEX-ChR2-GFP was injected into SIn of ChAT-Cre mice. Whole-cell voltage clamp recordings were made from acute coronal ACtx brain slices while photostimulating ChR2-expressing SIn_{ACh} axons. (B-D) Immunoreactive ChR2-expressing SIn_{ACh} axons (green) around a pyramidal neuron labeled following whole-cell recording (red). (B) Axons surrounding the soma. (C) Axons surrounding the proximal trunk dendrite. (D) Axons surrounding a segment of apical dendrite in layer 1 of cortex. (E-H) Average (4 trials each) excitatory and inhibitory currents evoked in a pyramidal neuron through stimulation of SIn_{ACh} axons in normal ACSF (nACSF, E), ACSF containing NBQX, AP5, & atropine (F), NBQX, AP5, atropine, and GBZ (G), or NBQX, AP5, atropine, GBZ, and mecamylamine (H). (I) Peak excitatory and inhibitory currents evoked through stimulation of SIn_{ACh} axons in various pharmacological conditions for a population of neurons. (J) Onset times for excitatory and inhibitory currents (n = 12 neurons from 7 mice). The inset depicts at higher magnification a neuron's response to SIn_{ACh} stimulation at holding potentials of −70mV (grey) and 0mV (black). (K) Grand average of excitatory currents evoked through stimulation of SIn_{ACh} axons after applying NBQX, AP5, atropine, and GBZ. Lighter shade traces represent SEM (n = 8 neurons. Values are mean ± SEM.

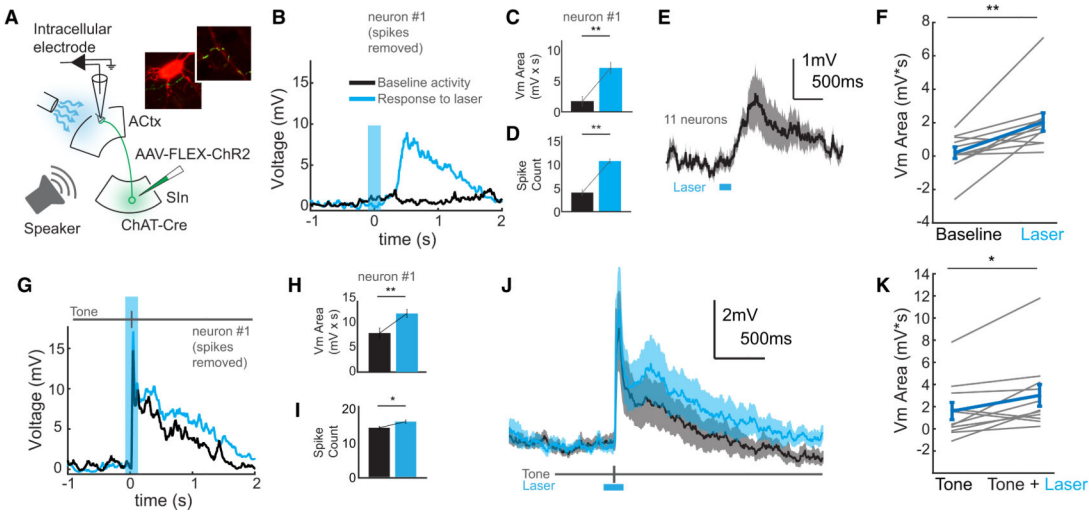

Figure 3. SIn_{ACh} Neurons Depolarize ACtx Neurons

(A) Schematic of the experimental strategy. AAV-FLEX-ChR2-GFP was injected into SIn of ChAT-Cre mice. Sharp intracellular current clamp recordings were made from mice while photostimulating ChR2-expressing SIn_{ACh} axons and playing sounds. The insets show ChR2-expressing SIn_{ACh} axons (green) around a pyramidal neuron labeled following intracellular recording (red). (B) Average response (20 trials, blue trace) to photostimulating SIn_{ACh} axons (blue shaded bar) for an example neuron. The black trace shows average response to blank stimulation trials. (C) Average voltage area following stimulation of SIn_{ACh} axons or blank trials for the example neuron in (B). (D) Average spike count following stimulation of SIn_{ACh} axons or blank trials for the example neuron in (B). (E) Grand average intracellular response to stimulation of SIn_{ACh} axons (n = 10 neurons from 3 mice). Shaded bounds indicate SEM. (F) Population depiction of evoked voltage area. The blue data points indicate the population mean and SEM. (G) Average response (40 trials) to tone playback alone (black trace) or tone playback with simultaneous photostimulation of SIn_{ACh} axons (blue trace) for the example neuron. (H) Mean voltage area in response to tone playback alone (black) or tone playback with stimulation of SIn_{ACh} axons (blue) for the example neuron. (I) Mean spiking response to tone playback alone (black) or tone playback with stimulation of SIn_{ACh} axons (blue) for the example neuron. (J) Grand average intracellular response to tone playback alone (black) or tone playback with stimulation of SIn_{ACh} axons (blue). Lighter shades depict SEM. (K) Population depiction of voltage area evoked to tone presentation alone or with stimulation of SIn_{ACh} axons. The blue data points indicate the population mean and SEM. Values are mean ± SEM.

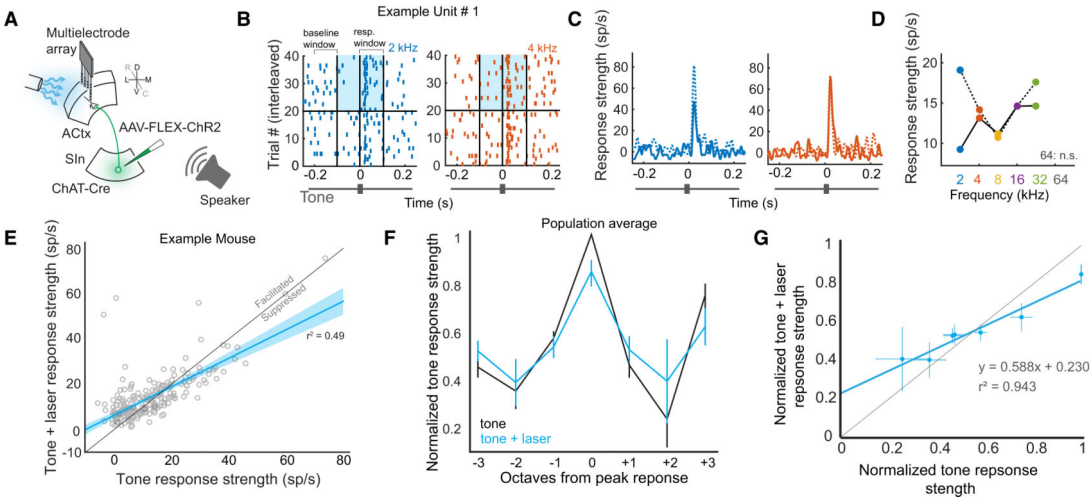

Figure 4. SIn_{ACh} Neurons Facilitate Weak and Suppress Strong Auditory Responses

(A) Schematic of the experimental strategy. AAV-FLEX-ChR2-GFP was injected into SIn of ChAT-Cre mice. Multielectrode extracellular recordings were made from ACtx while photostimulating ChR2-expressing SIn_{ACh} axons and playing sounds. (B) Raster plots for an isolated single unit in response to tone playback (2 kHz, blue or 4 kHz, orange) alone (bottom half), or with photostimulation of SIn_{ACh} axons (top half). The blue shaded box indicates the light stimulation period. (C) Peristimulus time histograms of response strength (RS) to tone stimulation alone (solid blue/orange traces), or tone + light stimulation (dashed blue/orange traces). (D) Tuning curve for the example unit without (solid trace) or with (dashed trace) stimulation of SIn_{ACh} axons. (E) Tone RS without light plotted against tone RS with light, for a single experiment. All significantly driven tone responses for each unit are included as individual data points. On average, tone responses are facilitated with light ($p = 0.0058$). The lighter blue shading indicates the functional prediction bounds for the linear regression. (F) Population tuning curve without (black) and with (blue) light stimulation (data are from 5 mice). (G) Population tone RS plotted against population tone + light RS for each group of responses (± 0, 1, 2, 3 octaves from peak response). The blue line is the linear fit. Values are mean ± SEM.

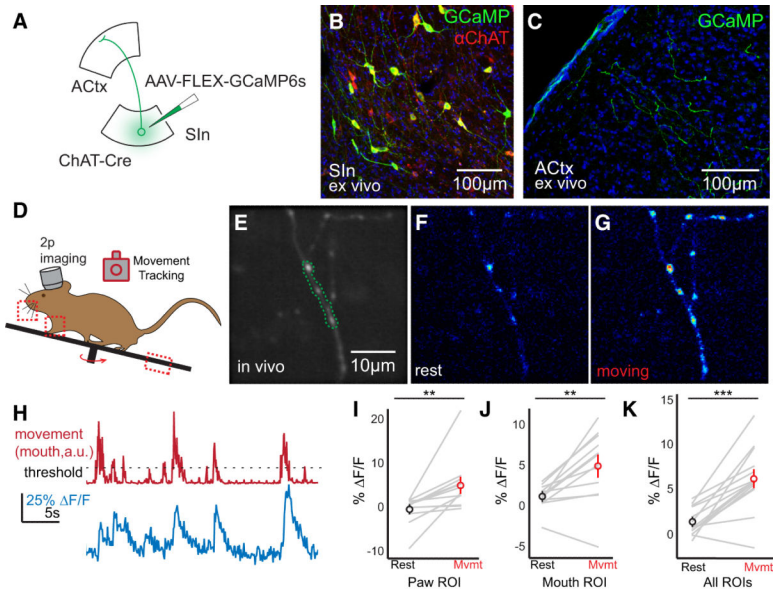

Figure 5. SIn_{ACh} Axons in ACtx are Active During Movements

(A) Schematic of the experimental strategy. AAV-FLEX-GCaMP6s was injected into SIn of ChAT-Cre mice. (B) Confocal micrograph of GCaMP-labeled SIn neurons. Neurons expressing GCaMP expressed ChAT (red). (C) Confocal micrograph of GCaMP-expressing SIn_{ACh} axons in ACtx. (D) Outline of experimental design for 2 photon imaging and tracking movements. ROIs for monitoring body movements are indicated with dashed boxes. (E) Average fluorescence of a GCaMP-labeled axon, imaged in vivo. The region outlined with a green dashed line indicates the ROI for monitoring changes in fluorescence over time. (F) Pseudocolored axonal fluorescence during rest. (G) Pseudocolored axonal fluorescence during a body movement. (H) ΔF/F from a single ROI (blue trace) during movements and rest (red trace). The dashed line indicates the threshold for identifying movements. (I) ΔF/F during paw movements (n = 12 axons, 2 mice). (J) ΔF/F during mouth movements (n = 12 axons, 2 mice). (K) ΔF/F during all body movements (n = 14 axons, 3 mice). (**p < 0.01, *** p < 0.001). Values are mean ± SEM.

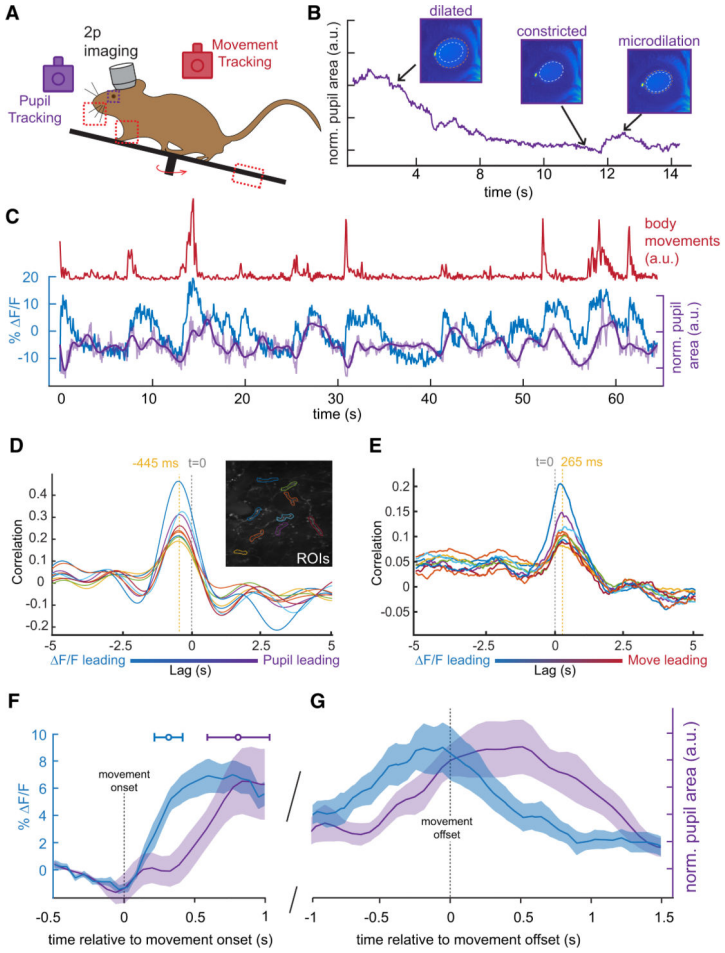

Figure 6. Movement-Related SIn_{ACh} Activity Precedes Pupil Microdilations

(A) Outline of experimental design for 2 photon imaging, tracking movements, and monitoring pupil size. (B) Changes in pupil size across time. Representative images from dilated, constricted, and microdilation periods are shown above. The dashed white circle corresponds to the size of the constricted pupil, while the orange circles illustrate the relative dilations. (C) ΔF/F from a single axon (blue) and pupil size (purple) during an epoch of small body movements (red). The lighter purple trace shows the unfiltered pupil size. (D) Cross correlation between ΔF/F of 9 ROIs and pupil microdilations. The lag between ΔF/F and pupil is indicated by the dashed orange line relative to time zero. The inset shows GCaMP labeling in SIn_{ACh} axons, and the ROIs selected for analysis. (E) Cross correlation between ΔF/F of the same ROIs from (D) and movement quantification. (F-G) Average and SEM of ΔF/F (blue trace, n = 14 imaging planes, 1 axon from each; 4 mice) and pupil area (purple trace, n = 5 imaging sessions, 2 mice) plotted with respect to movement onset (F) and movement offset (G). Values are mean ± SEM (shading), except for the horizontal error bars in (F), which represent SD.

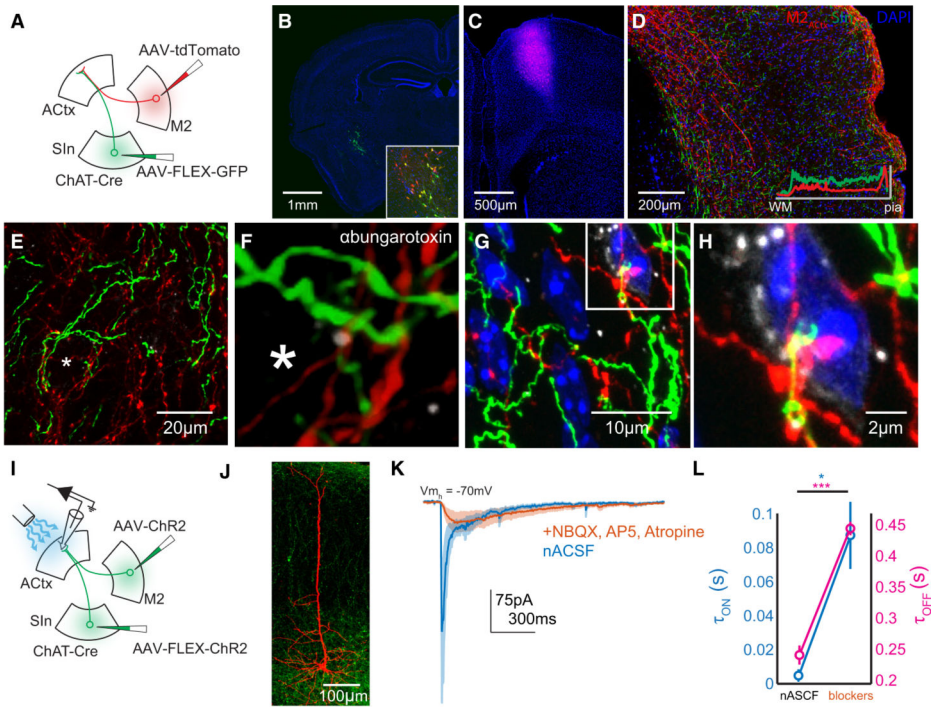

Figure 7. SIn_{ACh} and $M2_{ACtx}$ Synapses Converge on Single Auditory Cortical Neurons

(A) Schematic of the experimental strategy. AAV-FLEX-GFP was injected into SIn of ChAT-Cre mice. AAV-tdTomato was injected into the M2 of the same mice. (B) Confocal micrograph showing GFP labeling at the injection side. Blue is DAPI. The inset shows the injection site, immunostained for ChAT (red). (C) tdTomato labeling at the M2 injection site. (D) Labeling from SIn_{ACh} (green) and $M2_{ACtx}$ (red) axons in ACtx. The inset shows the fluorescence intensity of SIn_{ACh} and $M2_{ACtx}$ labeling across layers (averaged measurements from several brain sections). (E) Higher magnification Z stack showing SIn_{ACh} and $M2_{ACtx}$ axons near a putative cell body (asterisk). (F) Higher magnification image from (E). The Z stack was interpolated and rotated slightly. Nicotinic ACh receptors are labeled with α-bungarotoxin (greyscale). (G) Another Z stack showing SIn_{ACh} and $M2_{ACtx}$ axons near a cell body from a different mouse. DNA is labeled with DAPI. (H) Higher magnification Z stack from (G). (I) Schematic of the experimental strategy. AAV-FLEX-ChR2-GFP was injected into SIn of ChAT-Cre mice. AAVChR2-GFP was injected into the M2 of the same mice. Whole-cell voltage clamp recordings were made from acute coronal ACtx brain slices. (J) Confocal Z stack showing a pyramidal neuron labeled following whole-cell recording surrounded by ChR2-expressing axons. (K) Average traces of excitatory currents (5 neurons) in response to photostimulation of putative SIn_{ACh} and $M2_{ACtx}$ axons in normal ACSF (blue) and following application of blockers (orange; the shading indicates SEM). Nicotinic transmission is preserved after blocking glutamatergic $M2_{ACtx}$ currents. (L) Onset (blue) and offset (magenta) time constants of excitatory currents from (J).

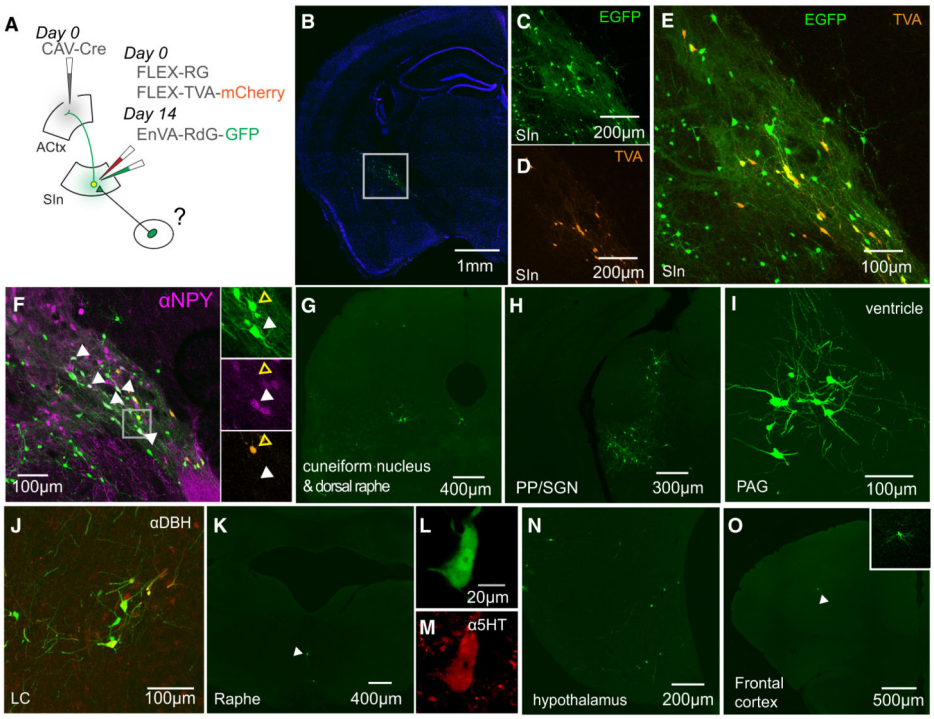

Figure 8. Synaptic Inputs to SIn_{ACtx} Neurons

(A) Schematic of the experimental strategy. On day 0, AAV-FLEX-RG and AAV-FLEX-TVA.mCherry were injected into SIn of wild type mice. Additionally, CAV-Cre was injected into ipsilateral ACtx. On Day 14, EnVA-RΔG.GFP is injected into SIn, which labeled neurons presynaptic to SIn_{ACtx} cells expressing TVA and RG. (B) GFP and TVA.mCherry labeling in SIn. (C) GFP-labeled SIn neurons. (D) TVA.mCherry-labeled SIn_{ACtx} neurons. (E) Overlaid images from (C) and (D). Neurons expressing both GFP and TVA.mCherry are starter cells. Neurons expressing GFP, but not mCherry, are putatively presynaptic to SIn_{ACtx} neurons. (F) A subset of SIn neurons putatively presynaptic to SIn_{ACtx} neurons stained positive for NPY (white arrowheads). The panels to the right show GFP (top), NPY (middle), and TVA.mCherry (bottom) labeling. The white arrowheads indicate a putative presynaptic ($GFP^+/TVA.mCherry^-$) neuron expressing NPY. The open yellow arrowhead indicates a starter cell ($GFP^+/TVA.mCherry^+$) not expressing NPY. (G-O) Neurons presynaptic to SIn neurons in cuneiform nucleus (G), peripeduncular nucleus and supragenicular nucleus (H), periaqueductal gray (I), locus coeruleus (J), raphe (K), hypothalamus (N), and frontal cortex (O).